Journal of Solid State Chemistry **164,** 339–344 (2002)
doi:10.1006/jssc.2001.9488, available online at http://www/idealibrary.com on IDEAL®

Solid Solutions of WO_3 into Zirconia in WO_3–ZrO_2 Catalysts

M. A. Cortés-Jácome,*,†,[1] J. A. Toledo-Antonio,* H. Armendáriz,* I. Hernández,† and X. Bokhimi‡

*Instituto Mexicano del Petróleo. Prog. Ingeniería Molecular, Eje Central L. Cárdenas # 152, 07730 México city D. F., México; †Universidad Autónoma Metropolitana-Azcapotzalco, Av. San Pablo # 180, Col. Reynosa Tamaulipas, 02200 México city D. F., México; and ‡Institute of Physics, National University of Mexico (UNAM), A. P. 20-364, 01000 México city D. F., México
E-mail: macortes@www.imp.mx

Received July 17, 2001; in revised form November 26, 2001; accepted December 21, 2001

Catalysts in the WO_3–ZrO_2 system were produced by coprecipitation of aqueous solutions of zirconium oxynitrate and ammonium metatungstate. Samples were characterized by X-ray powder diffraction, thermogravimetry, and refinement of their crystalline structures with the Rietveld method. This coprecipitation gave rise to solid solutions of tungsten oxide into zirconia; the initial phase was amorphous and crystallized into two tetragonal crystalline phases, T1 and T2, when samples were annealed at 560°C. The main difference between both phases was the oxygen position along the *c* axis. In the phase with higher symmetry, T2, an oxygen atom was at one-half of the unit cell, 0.50(2), producing flat crystallite surfaces perpendicular to the *c* axis, while in the phase with the lower symmetry, T1, it was at 0.447(2), and gave rise to rough crystallite surfaces parallel to (100) planes. The interpenetrating tetrahedra forming the representative polyhedron of the crystalline structure were almost nondeformed in the phase with higher symmetry, because all Zr–O atom bond lengths were very similar. As the annealing temperature of the sample was increased, the dissolved tungsten atoms in the phase with higher symmetry segregated to the crystallite's surface.

Key Words: **tungsten oxide; zirconium oxide solid solution; tetragonal zirconia; coprecipitation; XRD–Rietveld analysis.**

INTRODUCTION

Tungsten oxide dispersed on zirconia in the WO_3–ZrO_2 system gives rise to catalysts with strong acidic properties [1–5]. Like sulfated zirconia, it is able to isomerize *n*-alkanes at very low temperatures, but it has additional advantages, for instance, a higher thermal stability and resistance in H_2, O_2, and H_2O atmospheres (3, 4). Therefore, WO_3–ZrO_2 catalysts do not produce corrosive volatile compounds, and can be completely regenerated; this is the case in hydrocarbon isomerization and alkylation processes (1, 6), which are reactions of great interest for producing octane-enhancing additives to gasoline pools. These characteristics point out tungsten–zirconia catalysts as benchmark materials for the future (7).

Recently, WO_3–ZrO_2 catalysts have been studied intensively in order to explain their strong acid site density. The activation of the catalytic sites depends on the synthesis method, which also determines their convenient annealing temperature; for instance, when coprecipitation (4) and sol–gel (8) methods are used, for this activation annealing temperatures higher than that for impregnation in hydrous zirconia are required (9). It has been assumed that for impregnated catalysts all tungsten is on a crystallite surface, whereas in coprecipitated and sol–gel synthesis methods WO_3 crystallites remain in ZrO_2 bulk, stabilizing the tetragonal structure. This last synthesis method requires higher temperatures to segregate tungsten oxide on its surface, yielding catalysts with twice as high the acid site density obtained in the catalysts prepared by impregnation (8).

The high acid site density has been also explained by assuming that zirconia crystallites are covered with a WO_3 monolayer, when it is calcined between 800 and 850°C, depending on the tungsten oxide concentration (10–12). When the tungsten content is higher than the ideal amount for producing only one monolayer, it is assumed that three-dimensional growing of WO_x species (13), domains of WO_x with distorted octahedral symmetry, are supposed to be responsible for the high isomerization activity when compared with the tetrahedral species in WO_x/Al_2O_3 (14).

The above models only consider that WO_3 crystallites interact with ZrO_2 at surface layers. The possibility of a solid solution between these two oxides has not been contemplated until now, as when zirconia is stabilized with Ca, Cu, Y, La, or Ce (15, 16).

In the present work, it is shown that tungsten oxide and zirconia form solid solutions, stabilizing the tetragonal phase of zirconia. Samples were characterized by X-ray powder diffraction, thermoanalysis, and refinement of their crystalline structures.

[1]To whom correspondence should be addressed.

0022-4596/02 $35.00

EXPERIMENTAL

Synthesis. WO_3–ZrO_2 catalysts were prepared from zirconium oxynitrate, $ZrO(NO_3)_2 \cdot 6H_2O$ (Aldrich 99%), and ammonium metatungstate, $(NH_4)_6W_{12}O_{39} \cdot xH_2O$ (Aldrich 99%) as precursors; each was dissolved in water (0.17M). pH was maintained with an aqueous solution of ammonium hydroxide 14 vol%, NH_4OH (J. T. Baker, 28 vol%). The ammonium metatungstate solution was placed a 2000-ml container and the other two solutions were added slowly at the same rate in order to maintain the pH in the range of 9.5–10.0. The white gel obtained was aged for 24 h and dried at 110°C in a vacuum for 18 h; before characterization, dried powders were annealed at 560, 700, or 800°C.

Characterization. X-ray diffraction patterns of the samples packed in a glass holder were recorded at room temperature with Cu$K\alpha$ radiation in a Bruker Advance D-8 diffractometer having theta–theta configuration and a graphite secondary-beam monochromator. Diffraction intensity was measured in the 2Θ range between 15° and 110°, with a 2Θ step of 0.02° for 8 s per point. Crystalline structures were refined with the Rietveld technique by using DBWS-9411 (17) and FULLPROF-V3.5d (18) codes; peak profiles modeled with a pseudo-Voigt function (19) contained average crystallite size as one of its characteristic parameters (20). Standard deviations, which show the last figure variation of a number, are given in parentheses; when they correspond to Rietveld refined parameters, their values are not estimates of the probable error in the analysis as a whole, but only of the minimum possible errors based on their normal distribution (21).

Thermoanalysis. Weight loss curves were determined by thermogravimetry with a Perkin-Elmer TG-7 in the as-synthesized sample, which was heated from room temperature up to 1100°C at 5°C/min in air flowing at 20 cm^3/min.

Chemical composition. The chemical determination of tungsten in the annealed samples was made by atomic absorption spectroscopy with a Perkin-Elmer 2380 apparatus.

RESULTS AND DISCUSSION

After synthesis, samples were amorphous and crystallized when they were annealed in air at 560°C (Figs. 1 and 2). The TGA curve of the samples had four weight loss stages: one of 6.39 wt% and another of 5.56 wt% occurring below 200°C, which correspond to the desorption of the water molecules adsorbed on particles, surface. The others two weight loss stages, one of 6.03 wt% and another of 7.31 wt% occurring at 250 and 375°C, respectively, correspond to sample dehydroxilation. The two stages of dehydroxilation suggest the formation of two kinds of amorphous particles during synthesis, which were transformed into the two observed crystalline phases after annealing the sample, as will be evident from the X-ray analysis. The sample remained stable when it was annealed above 550°C; therefore, at above this temperature the crystalline phases did not have any transformation related to a weight loss.

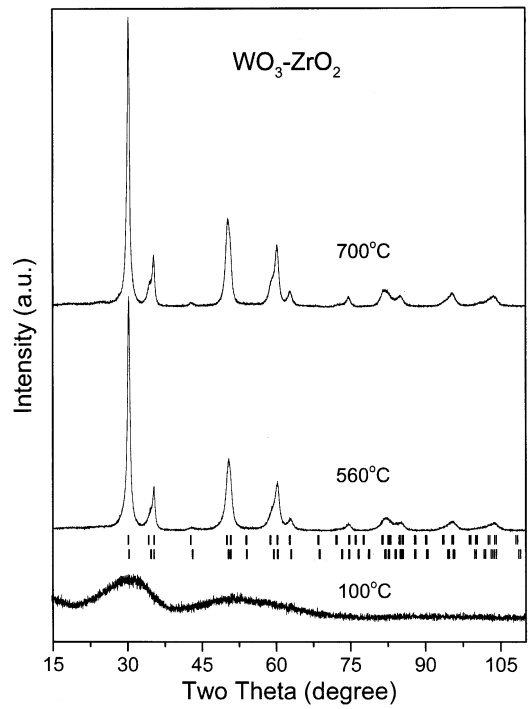

FIG. 1. X-ray diffraction patterns of WO_3–ZrO_2 samples annealed at temperatures between 100 and 700°C. Upper tick marks correspond to the tetragonal T1 phase and the lower ones to the tetragonal T2 phase. For clarity, the diffraction pattern of the amorphous phase was amplified.

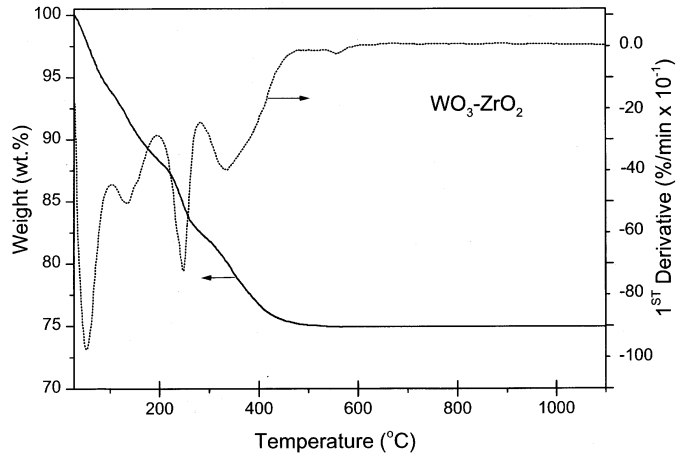

FIG. 2. TGA curve and its first derivative of the WO_3–ZrO_2 fresh sample.

TABLE 1
Tetragonal Zirconia (Space Group $P4_2/nmc$): Atomic Fractional Coordinates

Atom	Site	x	y	z
Zr	2a	0.75	0.25	0.25
W	2a	0.75	0.25	0.25
O	4d	0.25	0.25	u

The crystalline samples were composed of two tetragonal phases that had the same unit cell symmetry and similar lattice parameters, but different oxygen atom positions and atom bond lengths. Unit cell symmetry was described with space group $P4_2/nmc$, and had atoms in the positions given in Tables 1 and 2. This unit cell was used in the model of the X-ray diffraction pattern for refining the crystalline structures with the Rietveld method; Fig. 3 displays a typical refinement plot.

Elemental analysis of the samples by atomic absorption registered 14.6 wt% of WO_3. Both, the fact that the X-ray diffraction patterns (Fig. 1) were similar to those of tetragonal zirconia (22, 23) and that tungsten was in the samples clearly evidence that zirconia and tungsten oxide formed solid solutions. If that were not the case, other phases related with so large amounts of tungsten oxide would appear in the diffraction patterns, and the tetragonal phase would not be stable at so large annealing temperatures.

In the initial trial of refinement, the X-ray diffraction pattern of the sample annealed at 560°C was modeled with only one tetragonal phase. The fit of this model to the experimental data was bad, which suggested that the diffraction pattern contained more than one crystalline phase. Therefore, the diffraction pattern was analyzed with two different models, each containing two crystalline phases. The first model supposed one tetragonal and one cubic phase, one having the symmetry of tetragonal zirconia and the other that of cubic zirconia. The second model contained two tetragonal phases, T1 and T2, having the same symmetry as tetragonal zirconia; the best result was obtained for the second model. In order to enhance the findings, the results found in the sample crystallized at 560°C will be described in detail in the following paragraphs.

TABLE 2
Oxygen Position u in the Two Tetragonal Phases

T (°C)	T1	T2
560	0.447(2)	0.50(2)
700	0.456(3)	0.474(6)
800	0.452(2)	—

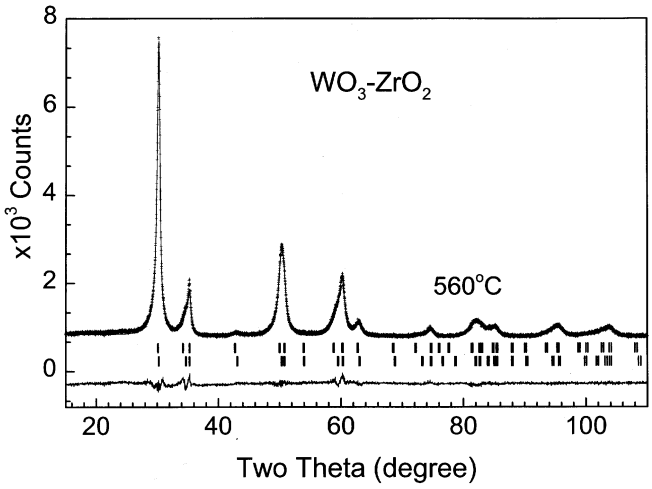

FIG. 3. Rietveld refinement plot of the sample annealed at 560°C ($R_{wp}=0.118$). Crosses correspond to the experimental data, and the continuous line to those calculated. The difference between experimental and calculated data is also shown with a continuous line. Upper tick marks correspond to the T1 phase ($R_B=0.034$) and the lower ones to T2 ($R_B=0.025$).

The refinement of the crystalline phases gave a concentration of 59(2) wt% for phase T1 and 41(1) wt% for T2 (Table 3). The corresponding average crystallite size was 6.3(2) and 44(3) nm, respectively. It is worth noting, that the lattice parameter a in both phases was almost equal, but they had different c lattice parameters (Table 4); more important was the fact that the corresponding oxygen atom positions were different (Table 2). Both differences are more evident by analyzing the unit cells (Fig. 4) and drawing the lattices with the oxygen polyhedra characteristic of tetrahedral zirconia (Figs. 5–7).

The unit cell of phase T2 was more symmetric than that of T1 (Fig. 4). This symmetry is determined by oxygen position along the c axis (Table 2): In T1 this position was 0.447(2), deforming the characteristic polyhedron, as evident from Fig. 4, which is a projection of the unit cell perpendicular to the b axis. This effect is amplified if many unit cells are brought together to build the lattice, and the corresponding oxygen polyhedra are shown (Fig. 5). The polyhedra deformation gives rise to crystallite surface

TABLE 3
Crystallite Size and Phase Composition

T(°C)	Phase	Composition (wt%)	Crystallite size (nm)
560	T1	59(2)	6.3(2)
560	T2	41(1)	44(3)
700	T1	63(5)	10.9(2)
700	T2	37(1)	34(1)
800	T1	63.4(4)	23.2(4)

TABLE 4
Lattice Parameters

T(°C)	Phase	a (nm)	c (nm)
560	T1	0.35924(8)	0.5236(2)
	T2	0.35936(6)	0.5167(1)
700	T1	0.35933(4)	0.5221(1)
	T2	0.35925(6)	0.5163(1)
800	T1	0.35953(3)	0.51885(5)

roughness as shown in the projections of the crystallite perpendicular to the a and c axes, which explains the reported roughness, observed with high-resolution transmission electron microscopy, for sulfated tetragonal zirconia on crystallite surfaces parallel to (100) planes (24). This roughness almost disappears in T2 (Fig. 6); this is more evident for the surface perpendicular to the c axis. The unit cell of this phase is much more symmetric because the position of the oxygen atom along the c axis (Fig. 4 and Table 2) was one half of it, 0.50(2). This high symmetry produced flat-surface crystallites (Fig. 6). The difference in crystallite surface roughness observed for T1 and T2 should play an important role when these materials are used in catalysis. Besides, the substitution of tungsten for zirconium in the lattice generates cationic and anionic vacancies that could be responsible of catalytic reactions; for example, CH_4 and CO oxidation (15).

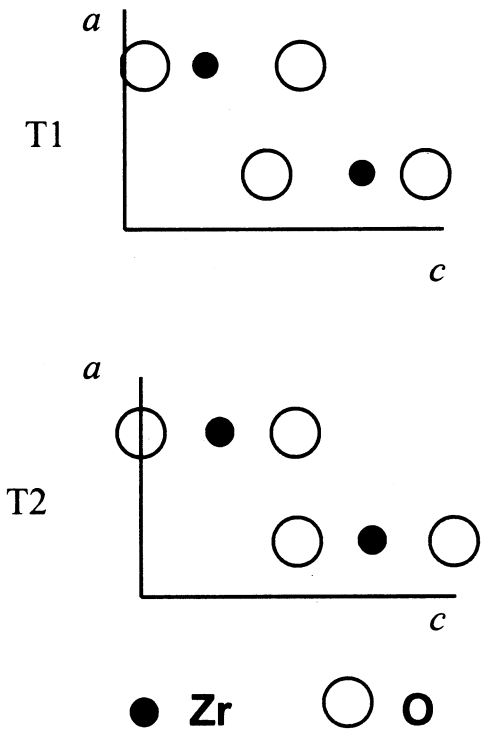

FIG. 4. Unit cell projection perpendicular to the b axis for both the T1 and T2 phases.

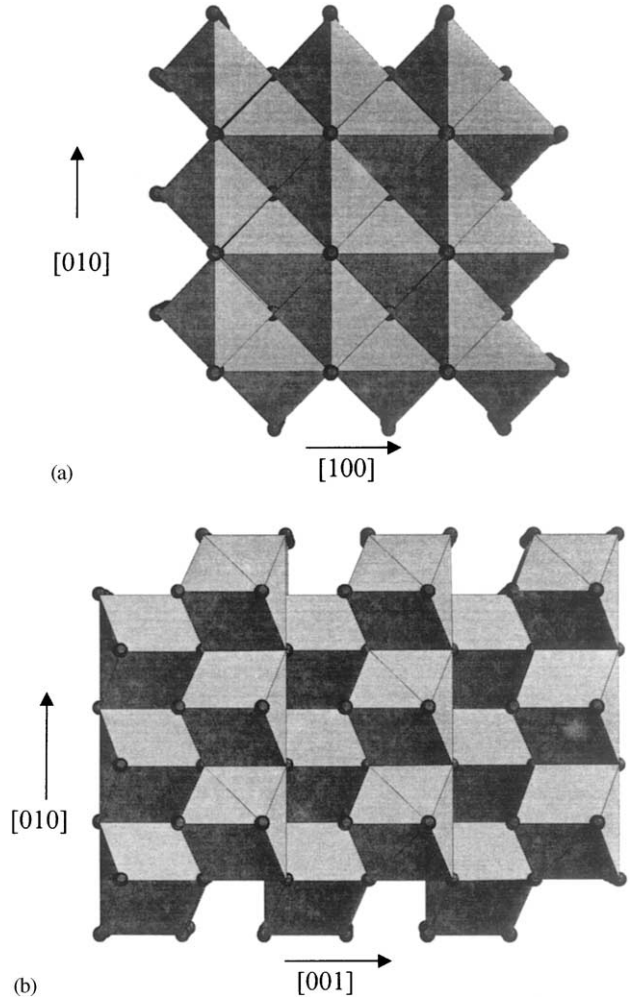

FIG. 5. Lattice of T1 phase: (a) projected perpendicular to the c axis, and (b) projected perpendicular to the a axis.

Analysis of the representative polyhedron of tetragonal zirconia (Fig. 7) shows that it is composed of two interpenetrating deformed tetrahedra. When the tetragonal symmetry tended to be cubic ($\sqrt{2}a \cong c$), as in T2, the tetrahedra were not more deformed, ϕ and δ were around 109° (Table 5), and the characteristic Zr–O bond lengths d_1 and d_2 were similar.

When the sample annealing temperature was increased to 700°C the difference between the crystallographic parameters of T1 and T2 was smaller (Tables 2 and 4). The symmetry of both phases tended to be the same; T2 lost its high symmetry, suggesting that its tungsten content decreased. A careful analysis of the diffraction pattern of the sample annealed at this temperature shows the presence of very weak peaks that can be associated with tungsten oxide, which was more evident when the sample was annealed at 800°C (Fig. 8). This suggests that part of the tungsten dissolved in the phase T2 of the sample annealed

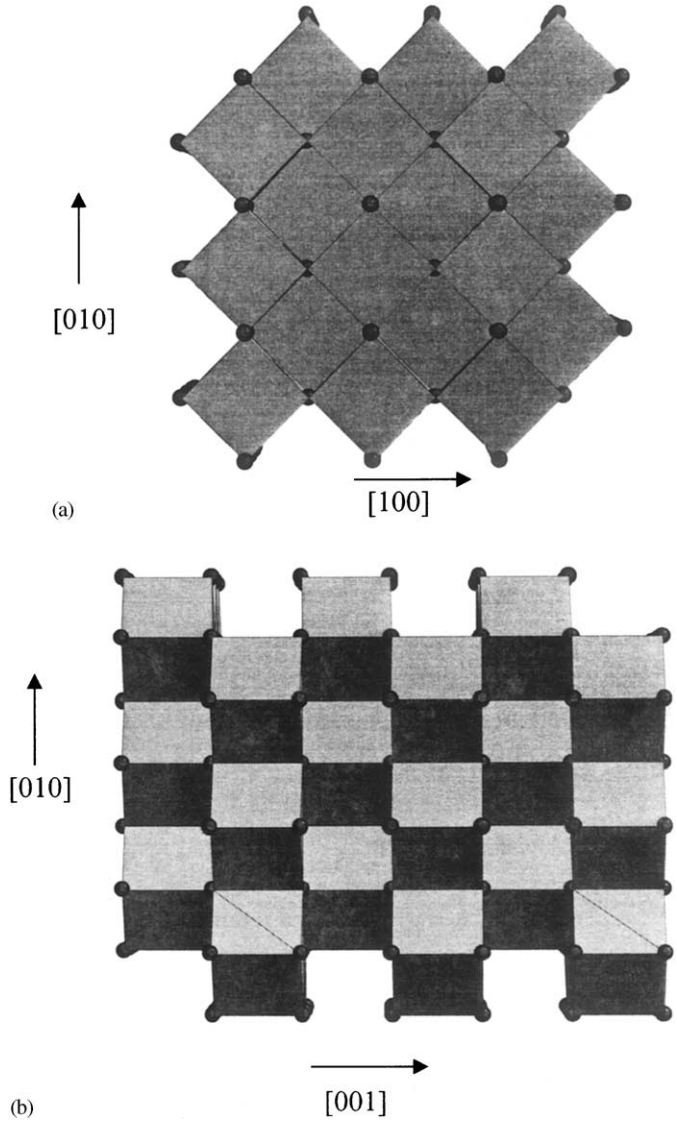

FIG. 6. Lattice of T2 phase: (a) projected perpendicular to the *c* axis, and (b) projected perpendicular to the *a* axis.

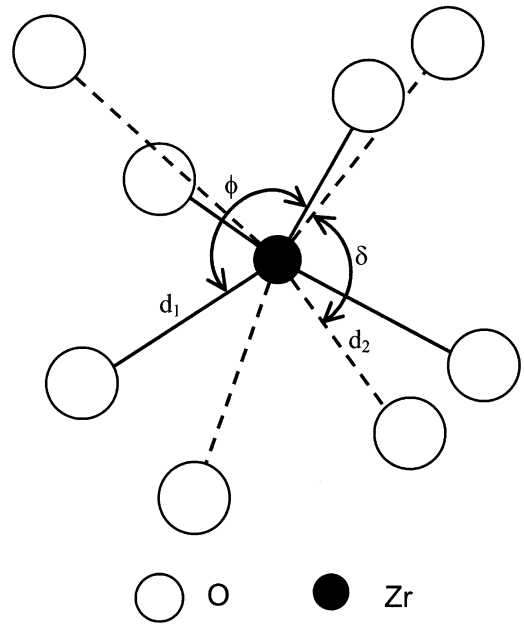

FIG. 7. Representative polyhedron of the tetragonal crystalline structure of zirconia; the two interpenetrating tetrahedra are clearly shown.

at 560°C segregated to the crystallite surface, which explains the observation by high-resolution electron microscopy of tungsten oxide surrounding crystallites in the WO_3–ZrO_2 system (25). This segregation broke the crystallites of phase T2, giving rise to a smaller average crystallite size: It changed from 44(3) to 34(1) nm (Table 3).

In contrast to the samples annealed at 560 and 700°C, those annealed at 800°C had only one tetragonal phase, which had approximately the same concentration as T1. It is worth noting that despite the high annealing temperature, the concentration of tetragonal phase was 63.4(4) wt% (Fig. 8). This phase coexisted with monoclinic zirconia and WO_3, which had concentrations of 25(2) and 11.3(5) wt% and crystallite sizes of 18(1) and 5.3(4) nm, respectively. For the refinement, monoclinic zirconia was modeled with a unit cell that had the symmetry of space group $P2_1/c$ (22), while WO_3 was modeled with an orthorhombic unit cell that had the symmetry of space group *Pmnb* (26).

To determine the WO_3 concentration in the T1 and T2 phases we started from the total WO_3 concentration in the sample measured by atomic absorption, which was 14.6 wt%. Since the crystallography of the T1 phase were almost temperature independent, it will be assumed that in this phase the WO_3 did not change. When the sample was annealed at 800°C, however, phase T2 was transformed into two phases: monoclinic zirconia and orthorhombic WO_3; the Rietveld refinement gave for this tungsten oxide a concentration of 11.3(5) wt% relative to the total number of phases in the sample (T1, monoclinic zirconia, and WO_3). The difference between the concentration of WO_3 determined via Rietveld refinement after annealing the sample at 800°C, and the WO_3 concentration measured by atomic adsorption in the sample was then 3.3 wt%, which should be in phase T1.

Since the concentration of the T1 phase in the sample was of 63.4(4) wt%, the above 3.3 wt% WO_3 concentration in the sample corresponds to a concentration of 2.8 mol% of WO_3 in the T1 phase, W/Zr = 0.027 atomic ratio. The WO_3 concentration of 11.3(5) wt% measured in the sample after it was annealed at 800°C corresponds to a concentration of 19.4 mol % of WO_3 in the T2 phase, W/Zr = 0.24 atomic ratio, which is on the same order as the copper concentration for stabilizing cubic zirconia (15).

TABLE 5
Atomic Bond Lengths and Bond Angles

T(°C)	Phase	d_1 (nm)	d_2 (nm)	ϕ	δ
560	T1	0.2071(6)	0.23960(6)	120.86(2)	116.22(2)
	T2	0.22084(6)	0.22174(6)	109.62(2)	108.00(2)
700	T1	0.20946(6)	0.23624(6)	118.14(2)	114.94(2)
	T2	0.21364(6)	0.22928(6)	114.45(2)	112.72(2)
800	T1	0.20806(6)	0.23715(6)	119.53(2)	115.18(2)

CONCLUSIONS

Coprecipitation of zirconium oxynitrate and ammonium metatungstate in aqueous solutions produced solid solutions of tungsten oxide into zirconia. The initial phase was amorphous and crystallized into two tetragonal crystalline phases, T1 and T2, when the samples were annealed at 560°C. The most important difference between both phases was the oxygen position along the c axis; in the phase with higher symmetry, T2, the oxygen atom was at one-half of the unit cell, 0.50(2), while in phase T1 it was at 0.447(2). This gave rise to rough and flat crystallite surfaces perpendicular to the c axis, for phases T1 and T2, respectively, which would be of big interest in catalysis. The interpenetrating tetrahedra forming the representative polyhedron of the crystalline structure were almost nondeformed in the phase with higher symmetry, because all Zr–O atom bond lengths were very similar. As the annealing temperature of the sample was increased, the dissolved tungsten atoms in the phase with higher symmetry segregated to the crystallite surface.

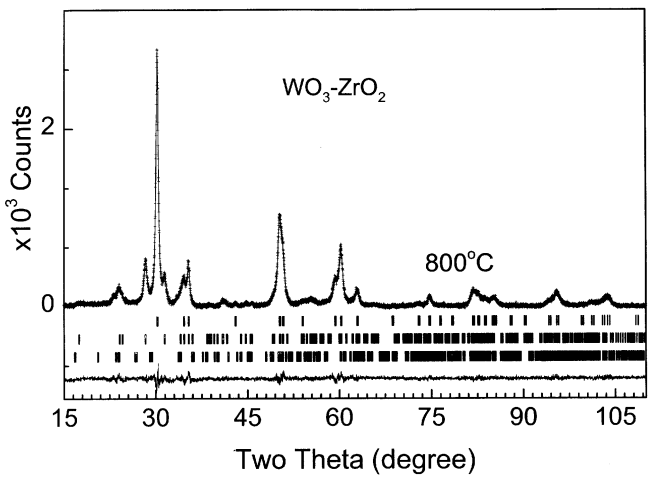

FIG. 8. Rietveld refinement plot of the sample annealed at 800°C ($R_{wp}=0.147$). Crosses correspond to the experimental data, and the continuous line to those calculated. The difference between experimental and calculated data is also shown with a continuous line. Upper tick marks correspond to the T1 phase ($R_B=0.017$), middle tick marks to monoclinic zirconia ($R_B=0.039$), and the lower ones to orthorhombic WO_3 ($R_B=0.066$).

ACKNOWLEDGMENTS

We thank Mr. Manuel Aguilar for his technical assistance. This work was financially supported via Grants IMP-D.01234 and IMP-FIES D.00065. M.A.C.J. warmly thanks the CONACYT of México for a grant.

REFERENCES

1. M. Hino and K. Arata, *J. Chem. Soc. Chem. Commun.* 1259 (1987).
2. K. Arata and M. Hino, *in* "Proc. 9th International Congress on Catalysis, Calgary, 1988" (M. J. Phillips and M. Ternan, Eds.), p. 1727. Chem. Institute of Canada, Ottawa, 1988.
3. E. Iglesia, D. G. Barton, S. L. Soled, S. Miseo, J. E. Baumgartner, W. E. Gates, G. A. Fuentes, and G. D. Meitzner, *in* "Proc. 11th Inter. Congr. Catal. 40th Anniversary, Studies in Surf. Sci. and Catal." (J. W. Hightower, W. N. Delgass, E. Iglesia, and A. T. Bell, Eds.) Elsevier, Amsterdam, 1996.
4. J. G. Santiesteban, J. C. Vartulli, S. Han, R. D. Bastian, and C. D. Chang, *J. Catal.* **168,** 431 (1997).
5. M. Scheithauer, T. K. Cheung, R. E. Jentoft, R. K. Grasselli, B. C. Gates, and H. Knözinger, *J. Catal.* **180,** 1 (1998).
6. G. Larsen, E. Lotero, R. D. Parra, L. M. Petkovic, H. S. Silva, and S. Raghavan, *Appl. Catal.* A **130,** 123 (1995).
7. R. A. Boyse and E. I. Ko, *Appl. Catal. A* **177,** L171 (1999).
8. R. A. Boyse and E. I. Ko, *J. Catal.* **171,** 191 (1997).
9. S. R. Vaudagna, S. A. Canavese, R. A. Comelli, and N. S. Fígoli, *Appl. Catal. A* **168,** 93 (1998).
10. D. G. Barton, S. L. Soled, G. D. Meitzner, G. A. Fuentes, and E. Iglesia, *J. Catal.* **181,** 57 (1999).
11. D. G. Barton, M. Shtein, R. D. Wilson, S. L. Soled, and E. Iglesia, *J. Phys. Chem. B* **103,** 630 (1999).
12. C. D. Baertsch, S. L. Soled, and E. Iglesia, *J. Phys. Chem. B* **105,** 1320 (2001).
13. K. C. Pratt, J. V. Sanders, and V. Christov, *J. Catal.* **124,** 416 (1990).
14. J. A. Horsley, I. E. Wachs, J. M. Brown, G. H. Via, and F. D. Hardcastle, *J. Phys. Chem. B* **91,** 4014 (1987).
15. M. K. Dongare, V. Ramaswamy, C. S. Gopinath, A. V. Ramaswamy, S. Scheurell, M. Brueckner, and E. Kemnitz, *J. Catal.* **199,** 209 (2001).
16. X. Bokhimi, A. Morales, A. García-Ruiz, T. D. Xiao, H. Chen, and P. R. Strutt, *J. Solid State Chem.* **142,** 409 (1999).
17. R. A. Young, A. Sakthivel, T. S. Moss, and C. O. Paiva-Santos, *J. Appl. Crystallogr.* **28,** 366 (1995).
18. J. Rodríguez-Carbajal, Laboratoire Leon Brillouin (CEA-CNRS), France.
19. P. Thompson, D. E. Cox, and J. B. Hasting, *J. Appl. Crystallogr.* **20,** 79 (1987).
20. R. A. Young and P. Desai, *Arch. Nauki Mat.* **10,** 71 (1989).
21. E. Prince, *J. Appl. Crystallogr.* **14,** 157 (1981).
22. X. Bokhimi, A. Morales, O. Novaro, M. Portilla, T. López, F. Tzompantzi, and R. Gómez, *J. Solid State Chem.* **135,** 28 (1998).
23. M. Pérez, H. Armendáriz, J. A. Toledo, A. Vázquez, J. Navarrete, A. Montoya, and A. García, *J. Mol. Catal. A* **149,** 169 (1999).
24. M. Benaïssa, J. G. Santiesteban, G. Diaz, C. D. Chang, and M. J. Yacaman, *J. Catal.* **161,** 694 (1996).
25. R. Perez, private communication.
26. E. Salje, *Acta Crystallogr. Sect. B* **24,** 1968 (1982).